Fermi National Accelerator Laboratory

FERMILAB-Pub-79/56-EXP
7120.381

(Submitted to Sov. J. Nucl. Phys.)

PROTON-PROTON DIFFRACTION DISSOCIATION AT VERY SMALL $|t|$ FOR INCIDENT MOMENTA 50-400 GeV/c

E. Jenkins
University of Arizona
Tucson, Arizona 85721 USA

and

A. Kuznetsov, B. Morosov, V. Nikitin, P. Nomokonov,
Y. Pilipenko, A. Sandacz, V. Smirnov,
and G. Takhtamyshev
Joint Institute for Nuclear Research
Dubna, USSR

and

E. Malamud and R. Yamada
Fermi National Accelerator Laboratory
Batavia, Illinois 60510 USA

and

D. Gross
University of Rochester
Rochester, New York 14627 USA

July 1979

Operated by Universities Research Association Inc. under contract with the Energy Research and Development Administrati

PROTON-PROTON DIFFRACTION DISSOCIATION AT VERY SMALL $|t|$ FOR INCIDENT MOMENTA 50-400 GeV/c

E. Jenkins
University of Arizona
Tucson, Arizona 85721 USA

and

A. Kuznetsov, B. Morosov, V. Nikitin, P. Nomokonov,
Y. Pilipenko, A. Sandacz,* V. Smirnov,
and G. Takhtamyshev
Joint Institute for Nuclear Research
Dubna, USSR

and

E. Malamud and R. Yamada
Fermi National Accelerator Laboratory
Batavia, Illinois 60510 USA

and

D. Gross†
University of Rochester
Rochester, New York 14627 USA

*Present address: Institute of Nuclear Research
Warsaw, Poland.

†Present address: Fermi National Accelerator Laboratory
Batavia, Illinois 60510 USA

ABSTRACT

The differential cross section, $d^2\sigma/dtdM_x^2$, for the inclusive reaction $pp \rightarrow Xp$ has been measured in the ranges of $0.001 \leq |t| \leq 0.017$ $(GeV/c)^2$ and $1.2 \leq M_x^2 \leq 8.0$ GeV^2 for incident proton momenta from 50 to 400 GeV/c. We present the averaged values of $d^2\sigma/dtdM_x^2$ vs. t and M_x^2 from 150 to 400 GeV/c. The differential cross section has been parametrized by $d^2\sigma/dtdM_x^2(s,t,M_x^2) = (1 + C/s)\ A(M_x^2)\ \exp(b(M_x^2)\ (t + 0.01))$.

I. INTRODUCTION

The diffraction scattering of protons on protons, deuterium and helium has been studied at low - t in a series of experiments by the Dubna-USA collaboration. This paper reports on the results of a measurement of the differential cross section $d^2\sigma/dtdM_x^2$, for the inclusive reaction pp → Xp. The measurement has been performed at Fermilab by detecting slow-recoil protons from a hydrogen-gas-jet target intersecting the accelerator beam.

II. EXPERIMENTAL METHOD

The experimental setup was located in the Internal Target Area at Fermilab.

The circulating beam of the accelerator multiply intercepted the pulsing hydrogen-gas-target. The jet target had the following characteristics: the pulse duration was 100 msec, the quantity of pulses per cycle 3, the thickness 2×10^{-8} g/cm^2, the full width at half maximum 12 mm.

Slow-recoil protons were detected by the stacks of two Si detectors 6 to 10 mm in diameter. The thickness were 17 to 100 μm for front detectors and 200 to 1500 μm for rear detectors.

The detectors were mounted in the movable vacuum "ionguide" connected directly to the main ring chamber. The distance from the target to the detector array was 7.2 m. The "ionguide" with the detectors could vary over an angle of 0-140 mrad (from 90° to the

beam direction). We present data in a $|t|$ range of 0.001 to 0.017 $(GeV/c)^2$. The lower limits depend on background conditions, the upper limits on the thicknesses of the rear detectors.

The data were obtained at two sets of proton momenta:

1) 50, 160, 340 GeV/c and

2) 50, 270, 400 GeV/c

for twelve angle positions.

About 400,000 inelastic events were recorded for a running period of 160 hours.

The data were normalized using two permanently fixed detector stacks which measured elastic scattering at $|t| = 0.01$ $(GeV/c)^2$. The absolute values of the elastic differential cross section were taken from Ref. 1. The uncertainty of normalization was estimated to be ±2%.

The M_x^2 values were limited for incident proton momenta, 50, 160, 270, 340 and 400 GeV/c, respectively: 1.8; 3.4; 5.8; 7.0 and 8.1 GeV^2.

III. DETERMINATION OF THE DIFFERENTIAL CROSS SECTIONS $d^2\sigma/dtdM_x^2$ AND THE M_x^2 RESOLUTION

The missing mass squared, M_x^2, and the differential cross section, $d^2\sigma/dtdM_x^2$, are given by:

$$M_x^2 = M_p^2 + 2p_1\sqrt{|t|}\left[\sin - (1+\frac{M_p}{p_1})\ \frac{|t|}{2M_p}\right] \qquad (1)$$

$$\frac{d^2\sigma}{dt dM_x^2} = \frac{\pi}{P_1\sqrt{(\frac{t}{2M_p})^2 + |t|}} \quad \frac{\Delta N(t)}{\Delta t} \; \frac{1}{L \cdot \Delta\Omega} \tag{2}$$

where p_1 is the incident proton momentum, M_p the proton mass, t- the four momentum transfer squared ($|t| = 2M_pT$, where T is the kinetic energy of the recoil proton), θ - the recoil angle measured from 90°, Δt the bin width in t, $\Delta N(t)$ the number of particles recorded in the Δt interval, $\Delta\Omega$ the detector solid angle, and L the target-beam luminosity ($L = N_{e\ell}/(\frac{d\sigma}{d\Omega}\,\Delta\Omega_{e\ell})$).

Figures 1 and 2 illustrate the recoil kinematics of the $pp \to Xp$ reaction. The M_x^2 resolution depends on the resolution of p_1, t and θ. We have $\Delta p_1 = \pm 6$ GeV/c, $\Delta\theta = \pm 1.0$ mrad, $\Delta t = \pm 2 \times 10^{-4}$ $(\text{GeV/c})^2$. In our kinematic region the values of ΔM_x^2 are of the order of ± 0.1 GeV^2.

IV. BACKGROUND SUBTRACTION

Figure 3 shows the kinetic energy spectra of recoil particles recorded by a stack of Si detectors at an angle of 78 mrad (from 90°). The thickness of the front detector is 190 μm and the thickness of the rear detector - 1500 μm.

Three spectra are presented:

a) $p_1 = 400$ GeV/c. One can observe the elastic scattering peak and two enhancements which correspond to $M_x^2 \approx 1.95$ GeV^2 and $M_x^2 \approx 2.8$ GeV^2.

b) p_1 = 50 GeV/c. There are practically no inelastic events in this spectrum. Taking into account the resolution, the largest M_x^2 value is about 1.17 GeV^2.

c) p_1 = 150 GeV/c. This spectrum was recorded during the same time interval as spectra (a) and (b), 1 sec after that the first jet pulse terminated. This spectrum consists of the recoils of residual (not pumped-out) hydrogen.

The shape of the recoil spectra depends on three different beam-gas interaction regions:

1) The central jet region (about 2 mrad).

2) The region of diffused gas around the jet which is directly "seen" by the detectors and clearly limited by ionguide collimators (about 12 mrad).

3) The extensive region of diffused gas shielded from direct view of the detectors by various parts of the apparatus. This region can provide sources of secondary particles.

Let us consider the shape of spectrum (b) in Fig. 3 which has no inelastic events. A steeply decreasing background of low energy recoil particles is observed from 0 to 2 MeV. The intensity of this background is directly proportional to the thickness of the front detector and makes a significant contribution of particles other than protons. The protons having energy above 5.5 MeV penetrate into the rear detector. The ΔE-E identification begins to work, and the background steeply decreases. In the range from 8.3 to 13.5 MeV one observes the narrow elastic peak placed on the flat

pedestal of elastic recoils from the diffused gas. The height of the pedestal is greatly limited due to the ionguide collimators. Above 13.5 MeV the background is practically the same as in front of the elastic pedestal.

We compared many spectra of the (a), (b) and (c) types and drew two conclusions:

(1) The background level is directly proportional to the amount of diffused gas (but not to the central jet density);

(2) The shape and the size of the background are practically independent of the beam proton momentum.

Taking into account these conclusions we subtracted the 50 GeV/c spectra as background from the 160-400 GeV/c spectra. The 50 GeV/c data were slightly stretched to correct for small elastic kinematic differences at the two momenta and then normalized to the high momentum data so that the numbers of elastic counts were equal.

This method of background subtraction made it possible to use all parts of the spectra including the ranges, where the particles are not identified, and the ranges near the elastic peak. The procedure of subtraction does not work at the angles where the inelastic cross section at 50 GeV/c is sizable. For these ranges only particles stopping in the rear detectors were used, and the background, averaged over the region from the elastic pedestal to the pion threshold, was subtracted. This background was assumed to be constant and was equal to (taking into account Eq. (2)):

$$d^2\sigma/dtdM_x^2(p_1) = 1.2 \times 50/p_1 \quad \frac{mb}{(GeV/c)^2\ GeV^2}$$

This background can be seen in Fig. 3b in an interval of 5.5-8.3 MeV and in Fig. 4, where the differential cross section is shown at 50 GeV/c.

V. THE DEPENDENCE OF THE DIFFERENTIAL CROSS SECTION $d^2\sigma/dtdM_x^2$ ON INCIDENT PROTON MOMENTUM, p_1

The differential cross sections are fitted by the exponential form:

$$\frac{d^2\sigma}{dtdM_x^2}(p_1,M_x^2,t) = a(M_x^2,p_1)\exp(b(p_1, M_x^2)\ (t + 0.01)) \qquad (3)$$

(We use $(t + 0.01)$ instead of the usual (t) to decrease the a and b correlation. The value $t = -0.01\ (GeV/c)^2$ is approximately the center of our t-range).

At this step of data processing the choice of just the exponential dependence is not very important (because our t-range is very narrow, the fit is done mainly to get the average characteristics of our data set.)

Then the $a(p_1,M_x^2)$ is fitted by

$$a(p_1,M_x^2) = a_\infty(M_x^2)\left(1 + \frac{C(M_x^2)}{p_1}\right) \qquad (4)$$

The values of $a(p_1,M_x^2)$, $a_\infty(M_x^2)$ and $C(M_x^2)$ are presented in Table I.

The value of $C(M_x^2)$ is shown in Fig. 5. In a range of $1.3 \leq M_x^2 \leq 3.2$ Gev^2 the averaged C value is $\bar{C} = 19 \pm 4$ GeV/c.

Assuming this averaged dependence on p_1 for all data, we have

$$\frac{d^2\sigma}{dtdM_x^2}(p_1,M_x^2,t) = \left(1 + \frac{19\pm4}{p_1}\right)a_\infty(M_x^2)\exp(b(M_x^2)(t + 0.01)) \qquad (5)$$

The spread and the errors of $b(p_1,M_x^2)$ are large, and we do not present their values here. The values of $b(M_x^2)$ averaged over 160-400 GeV/c will be obtained below.

VI. M_x^2 AND t DEPENDENCE OF THE $d^2\sigma/dtdM_x^2$ CROSS SECTIONS

To have more information to study the M_x^2 and t dependence of $d^2\sigma/dtdM_x^2$, we combined the data at 160, 270, 340 and 400 GeV/c and normalized them to p_1 = 300 GeV/c according to Eq. 5:

$$\frac{d^2\sigma}{dtdM_x^2}\,(p_1 = 300\ \text{GeV/c}) = \frac{d^2\sigma}{dtdM_x^2}\,(p_1)\ \left(1 + \frac{19}{300}\right)\Big/\left(1 + \frac{19}{p_1}\right)$$

These normalized values of $d^2\sigma/dtdM_x^2$ are presented in Table II. Several examples of the t-dependence of $d^2\sigma/dtdM_x^2$ at fixed M_x^2 values are plotted in Fig. 6. Table II, and figures 7 and 8 show the values of $A(M_x^2)$ and $b(M_x^2)$ obtained by fitting

$$\frac{d^2\sigma}{dtdM_x^2}(t,M_x^2) = A(M_x^2)\exp(b(M_x^2)\ (t + 0.01)) \tag{6}$$

Typical values of χ^2 are 1.5 per degree of freedom. We do not show the $b(M_x^2)$ values for $M_x^2 > 3.2$ GeV^2 because the errors are very large. The data at $|t| < 0.003$ (GeV/c)^2 are not used for this fit as the Coulomb production of pions cannot be neglected at such small $|t|$.

We also present an empirical parametrization of $A(M_x^2)$ and $b(M_x^2)$.

$$A(M_x^2) = \left(1-\exp\left(-\left(\frac{M_x-M_o}{0.22}\right)^2\right)\right)\sum_{k=1}^{3} F_k(M_x) + \\ + C_4\left(1-\exp\left(-\left(\frac{M_x-M_o}{0.056}\right)^2\right)\right)\frac{1}{M_x^2} \tag{7}$$

where $M_o = M_p + M_\pi$, F_k are the Breit-Wigner type functions

$$F_k = C_k\,\Gamma_k^2/(M_x(4(M_x-M_k)^2 + \Gamma_k^2))^2 \tag{8}$$

$C_1 = 1.14 \pm 0.05$; $C_2 = 1.58 \pm 0.02$; $C_3 = 0.12 \pm 0.04$;

$C_4 = 4.64 \pm 0.10$;

$M_1 = 1.408 \pm 0.002$, $M_2 = 1.682 \pm 0.003$, $M_3 = 2.14 \pm 0.02$.

$\Gamma_1 = 0.356 \pm 0.007$, $\Gamma_2 = 0.216 \pm 0.013$. $\Gamma_3 = 0.33 \pm 0.10$.

$b(M_x^2)$ is parametrized by

$$b(M_x^2) = (13.2 \pm 1.2)\exp(-(0.74 \pm 0.30)\ (M_x^2 - M_o^2)^4) \\ + 6.5\ (\mathrm{GeV/c})^{-2}. \tag{9}$$

The asymptotic value $b(M_x^2 = \infty) = 6.5\ (\mathrm{GeV/c})^{-2}$ was not found by this fit but was taken from references 2 and 3.

VII. CONCLUSIONS

The results of this work can be summarized as follows:

1) The experimental method of the gas jet target together with recording recoils by solid state detectors works well for studying the reaction $pp \to Xp$ to $|t|$ as small as $|t| = 0.001\ (\mathrm{GeV/c})^2$.

2) The tables present the differential cross section $d^2\sigma/dtdM_x^2$ vs. t and M_x^2 averaged over 160-400 GeV/c in intervals of $1.2 \leq M_x^2 \leq 8.0\ \mathrm{GeV}^2$ and $0.001 \leq |t| \leq 0.017\ (\mathrm{GeV/c})^2$.

3) The differential cross section is parametrized by

$$\frac{d^2\sigma}{dtdM_x^2}(t,M_x^2) = A(M_x^2)\exp(b(M_x^2)\ (t + 0.01)).$$

The parameters $A(M_x^2)$ and $b(M_x^2)$ are approximated by empirical formulae (7) and (9).

4) The $b(M_x^2)$ values are in good agreement with data of other experiments on nucleon diffraction dissociation at larger $|t|$ values (for instance, references 4 and 5). This means that the exponential t-dependence of the differential cross section $d^2\sigma/dtdM_x^2$ holds down to $|t| = 0.002\ (\mathrm{GeV/c})^2$. No indication of a turnover is observed.

5) The differential cross section $d^2\sigma/dtdM_x^2$ shows a small energy dependence form 50 to 400 GeV.

The s-dependence, averaged in an interval of $1.2 \leq M_x^2 \leq 3.0$ GeV^2, is approximated by

$$\frac{d^2\sigma}{dtdM_x^2}(s, t, M_x^2) = \left(1 + \frac{36 \pm 8}{s}\right) a_\infty (t, M_x^2)$$

ACKNOWLEDGMENTS

We acknowledge the strong support of the Fermilab Internal Target Group led by Dr. T. Nash.

The Dubna members of the collaboration are very grateful to the Fermilab Directorate for support and hospitality during their stay.

This work was supported in part by the U.S. Department of Energy, the U.S. National Science Foundation and the U.S.S.R. State Committee for Atomic Energy.

REFERENCES

[1]D. Gross et al., Phys. Rev. Lett. 41, 217 (1978).

[2]Y. Akimov et al., Phys. Rev. Lett., 39, 1432 (1977).

[3]M. G. Albrow et al., Nucl. Phys. B108 1 (1976).

[4]H. De Kerret et al., Phys. Lett., 63B, 477 (1976).

[5]J. Biel et al., Phys. Rev. Lett., 36, 504-507; Phys. Lett., 65B, 291 (1976).

TABLE CAPTIONS

Table I: The values of $a(p_1, M_x^2)$ determined by the fit

$$\frac{d^2\sigma}{dtdM_x^2}(p_1, M_x^2, t) = a(p_1, M_x^2)\exp(b(p_1, M_x^2)\ (t + 0.01)).$$

The parameters C and a_∞ are determined by the fit

$$a(p_1, M_x^2) = a_\infty(M_x^2)\ \ 1 + \frac{C(M_x^2)}{p_1}$$

(The errors are statistical).

Table II: The differential cross section $d^2\sigma/dtdM_x^2$ obtained for p_1 equal to 160, 270, 340, 400 GeV/c and normalized to p_1 = 300 GeV/c according to Eq. 5; $A(M_x^2)$ and $b(M_x^2)$ are determined by the fit

$$\frac{d^2\sigma}{dtdM_x^2}(M_x^2, t) = A(M_x^2)\exp(b(M_x^2)\ (t + 0.01))$$

(The errors are statistical).

TABLE I

M_x^2 GeV^2	$a(P_1, M_x^2)$ mb/(GeV/c)^2 GeV^2 50 GeV/c	160 GeV/c	270 GeV/c	340 GeV/c	400 GeV/c	C GeV/c	a_∞ mb/(GeV/c)^2 GeV^2
1.2	2.40±0.40	1.85±0.16	1.55±0.21	1.75±0.17	0.99±0.19	50±17	1.30±0.14
1.3	3.42±0.30	3.04±0.11	2.99±0.15	2.87±0.11	2.59±0.12	17± 7	2.69±0.10
1.4	4.94±0.32	3.89±0.10	3.65±0.19	3.64±0.11	3.53±0.13	23± 5	3.38±0.10
1.5	5.23±0.44	4.53±0.13	4.70±0.35	4.40±0.16	4.27±0.13	13± 6	4.20±0.13
1.6	6.36±0.63	5.19±0.14	4.78±0.14	4.64±0.20	5.09±0.20	21± 7	4.56±0.17
1.7	7.32±0.57	5.60±0.15	5.76±0.16	5.76±0.15	5.91±0.25	10± 6	5.51±0.16
1.8	9.06±1.00	6.77±0.17	6.82±0.16	6.67±0.14	7.63±0.64	13± 7	6.44±0.21
1.9	-	7.61±0.13	7.07±0.21	7.17±0.14	7.30±0.20	19± 8	6.82±0.23
2.0	-	7.45±0.16	7.11±0.21	6.86±0.13	6.68±0.13	28± 9	5.36±0.42
2.1	-	6.67±0.19	6.54±0.16	6.26±0.14	6.03±0.13	31±11	5.70±0.23
2.2	-	5.65±0.22	5.70±0.15	5.19±0.12	5.15±0.12	36±14	4.76±0.23
2.3	-	4.50±0.40	4.41±0.30	4.48±0.18	4.18±0.20	26±28	4.00±0.35
2.4	-	3.91±0.40	3.84±0.11	3.51±0.10	3.52±0.11	67±32	3.00±0.30
2.5	-	3.70±0.35	3.40±0.10	3.22±0.10	3.31±0.14	46±32	2.89±0.31
2.6	-	3.50±0.40	3.28±0.11	3.08±0.11	3.30±0.13	23±33	3.00±0.30
2.7	-	3.69±0.34	3.37±0.12	3.02±0.11	3.30±0.12	51±32	2.80±0.30
2.8	-	-	3.38±0.16	3.16±0.12	3.10±0.11	100±70	2.46±0.50
2.9	-	-	3.27±0.14	3.00±0.16	3.08±0.16	96±76	2.40±0.60
3.0	-	3.21±0.41	2.79±0.10	2.43±0.10	2.57±0.10	114±48	1.93±0.30
3.1	-	2.67±0.30	2.70±0.20	2.23±0.10	2.24±0.10	80±42	1.82±0.26
3.2	-	-	2.14±0.10	1.91±0.10	2.12±0.10	29±65	1.90±0.40
3.8	-	1.41±0.36	1.30±0.20	1.28±0.20	1.38±0.30	19±90	1.23±0.43

TABLE II

M_x^2 GeV^2	$d^2\sigma/dtdM_x^2$ mb/(GeV/c)^2 GeV^2, 0.002 ≤ |t| ≤ 0.016 (GeV/c)^2								A mb/(GeV/c)^2 GeV^2	b (GeV/c)$^{-2}$
	0.002	0.004	0.006	0.008	0.010	0.012	0.014	0.016		
1.2	-	-	-	1.21±0.31	1.50+0.21	-	-	-	-	-
1.3	3.01±0.21	3.31±0.11	2.94±0.17	2.92±0.15	2.87±0.16	2.59±0.10	-	2.87±0.21	2.83±0.06	22.0±5.1
1.4	4.79±0.19	4.17±0.12	4.02±0.14	3.89±0.14	3.77±0.16	3.41±0.11	3.43±0.18	-	3.67±0.06	22.6±4.3
1.5	4.96±0.26	4.75±0.13	4.92±0.15	4.51±0.19	4.36±0.15	4.22±0.13	3.65±0.36	-	4.36±0.07	18.4±4.3
1.6	4.85±0.22	4.83±0.15	5.39±0.17	5.09±0.15	4.79±0.20	4.97±0.16	-	4.37±0.20	4.89±0.07	8.5±3.7
1.7	6.51±0.24	6.18±0.14	6.55±0.16	5.89±0.22	5.59±0.26	5.60±0.29	4.88±0.18	5.29±0.23	5.67±0.08	20.3±3.0
1.8	7.39±0.27	7.19±0.13	7.30±0.16	7.34±0.17	6.75±0.39	6.39±0.22	5.80±0.23	6.06±0.24	6.67±0.08	17.3±2.7
1.9	7.68±0.25	7.90±0.13	7.78±0.16	8.24±0.30	7.19±0.32	6.47±0.19	6.49±0.20	6.56±0.19	7.12±0.07	19.2±2.2
2.0	7.67±0.26	7.37±0.15	7.28±0.16	6.92±0.16	6.95±0.37	6.42±0.15	6.53±0.17	6.42±0.29	6.79±0.07	13.8±2.5
2.1	7.28±0.28	6.82±0.13	6.45±0.14	7.28±0.35	6.21±0.23	6.02±0.17	5.78±0.16	5.89±0.28	6.22±0.07	14.5±2.6
2.2	5.39±0.34	5.46±0.12	5.49±0.13	5.59±0.21	5.70±0.27	5.21±0.13	5.12±0.16	5.10±0.39	5.33±0.07	6.5±3.0
2.3	4.44±0.25	4.52±0.17	4.38±0.16	4.73±0.28	4.26±0.18	4.10±0.15	4.10±0.15	4.11±0.50	4.26±0.07	10.3±4.3
2.4	3.48±0.27	3.78±0.12	4.02±0.17	3.69±0.18	3.56±0.15	3.61±0.10	3.49±0.22	3.49±0.14	3.66±0.05	8.3±3.6
2.5	3.88±0.23	3.40±0.19	3.39±0.16	3.22±0.20	3.18±0.22	3.38±0.11	3.36±0.18	2.85±0.19	3.30±0.06	6.7±5.1
2.6	3.35±0.18	3.46±0.11	3.02±0.47	3.27±0.24	3.13±0.21	3.30±0.12	3.11±0.12	2.99±0.24	3.25±0.06	9.7±4.2
2.7	3.83±0.22	2.95±0.15	3.46±0.14	3.45±0.13	3.13±0.15	3.24±0.11	2.84±0.13	3.18±0.15	3.19±0.05	5.5±4.2
2.8	3.08±0.18	3.51±0.11	3.43±0.12	2.91±0.30	3.17±0.26	3.13±0.13	3.01±0.20	2.93±0.31	3.20±0.07	11.6±4.8
2.9	3.43±0.27	2.88±0.13	3.17±0.14	3.27±0.18	3.39±0.29	2.88±0.11	2.75±0.17	3.00±0.15	2.98±0.06	3.6±4.5
3.0	2.92±0.19	2.44±0.14	2.77±0.19	2.72±0.14	2.66±0.13	2.47±0.12	2.57±0.09	2.47±0.13	2.58±0.05	2.5±4.8
3.1	2.10±0.23	2.23±0.11	2.34±0.16	2.17±0.32	2.04±0.13	2.33±0.09	2.10±0.10	2.30±0.12	2.23±0.05	-
3.2	2.23±0.27	1.75±0.10	1.76±0.11	1.76±0.09	1.89±0.15	1.88±0.09	1.71±0.11	-	1.80±0.04	-

TABLE II continuation

M_x^2 GeV^2	$d^2\sigma/dtdM_x^2$ mb/(GeV/c)^2 GeV^2, 0.002 ≤ |t| ≤ 0.016 (GeV/c)^2								A mb/(GeV/c)^2 GeV^2	b (GeV/c)$^{-2}$
	0.002	0.004	0.006	0.008	0.010	0.012	0.014	0.016		
3.3	1.33±0.25	1.79±0.14	1.70±0.10	2.00±0.17	1.63±0.10	1.55±0.09	1.70±0.15	1.65±0.20	1.67±0.05	-
3.4	1.53±0.24	1.49±0.11	-	1.63±0.23	1.48±0.15	1.42±0.09	1.74±0.11	1.45±0.17	1.52±0.05	-
3.5	1.70±0.49	1.28±0.10	1.44±0.10	1.66±0.14	1.32±0.17	1.36±0.09	1.59±0.13	1.12±0.29	1.42±0.05	-
3.6	1.30±0.38	1.09±0.13	1.33±0.11	1.31±0.12	1.45±0.17	1.46±0.10	1.32±0.13	-	1.35±0.05	-
3.8	-	1.35±0.13	-	-	1.32±0.15	1.28±0.06	1.39±0.09	1.39±0.07	1.32±0.05	-
4.0	-	-	1.35±0.12	1.25±0.10	1.33±0.11	1.27±0.13	1.38±0.06	1.24±0.18	1.32±0.05	-
4.2	-	1.42±0.24	1.46±0.24	-	1.25±0.13	1.36±0.05	0.91±0.24	-	1.36±0.05	-
4.4	-	-	1.35±0.16	1.28±0.12	1.42±0.11	1.31±0.08	1.24±0.10	1.25±0.07	1.32±0.05	-
4.6	-	-	-	-	1.20±0.15	1.25±0.06	1.22±0.05	1.19±0.16	1.26±0.09	-
4.8	-	-	-	-	1.18±0.17	1.11±0.08	-	-	1.12±0.10	-
5.0	-	-	-	-	1.14±0.31	1.06±0.13	0.96±0.11	1.00±0.08	1.07±0.16	-
5.2	-	-	-	-	0.99±0.12	1.08±0.06	0.97±0.06	0.92±0.17	1.08±0.09	-
5.4	-	-	-	-	1.08±0.28	0.95±0.08	0.96±0.10	0.96±0.13	0.97±0.12	-
5.6	-	-	-	-	0.89±0.17	0.82±0.08	0.93±0.10	0.83±0.18	0.84±0.11	-
5.8	-	-	-	-	-	0.85±0.19	0.69±0.15	0.83±0.22	0.80±0.10	-
6.0	-	-	-	-	0.95±0.16	1.01±0.07	0.87±0.07	0.85±0.09	0.92±0.10	-
6.2	-	-	-	-	0.75±0.19	0.78±0.09	0.85±0.09	0.79±0.12	0.77±0.12	-
6.4	-	-	-	-	-	0.78±0.18	-	-	0.78±0.18	-
6.8	-	-	-	-	0.84±0.13	0.70±0.06	0.74±0.08	0.67±0.11	0.77±0.09	-
7.0	-	-	-	-	-	0.79±0.11	0.68±0.09	0.68±0.12	0.73±0.10	-
7.2	-	-	-	-	0.72±0.15	0.59±0.14	-	-	0.65±0.15	-
7.4	-	-	-	-	-	0.61±0.07	0.68±0.07	0.66±0.10	0.65±0.10	-
7.8	-	-	-	-	0.55±0.19	0.63±0.11	-	-	0.59±0.15	-
8.0	-	-	-	-	-	0.44±0.12	0.59±0.09	0.43±0.11	0.52±0.10	-

FIGURE CAPTIONS

Figure 1: Recoil kinematics for the inclusive reaction $pp \to Xp$ at 400 GeV/c beam momentum.
(θ is measured from 90° to the beam direction).

Figure 2: Missing mass kinematics at a fixed angle of 100 mrad for several values of the beam momentum.

Figure 3: Energy spectra of recoils observed by the detector stack at an angle of 78 mrad. The thickness of the front detector is 190 μm and the thickness of the rear detector 1500 μm. The dark line is the spectrum at 400 GeV/c. The light line is the spectrum at 50 GeV/c. The shaded spectrum is recorded from residual gas at 150 GeV/c. This figure is discussed in detail in the text.

Figure 4: Differential cross section $d^2\sigma/dtdM_x^2$ vs. M_x^2 at $|t| = 0.01\ (\mathrm{GeV/c})^2$ and $p_1 = 50$ GeV/c. The background is not subtracted.

Figure 5: Parameter $C(M_x^2)$ determined by the fit

$$\frac{d^2\sigma}{dtdM_x^2}(p_1, M_x^2, t) = 1 + \left(\frac{C(M_x^2)}{p_1}\right) a_\infty(M_x^2) \exp(b(p_1, M_x^2)\ (t + 0.01))$$

Figure 6: The $d^2\sigma/dtdM_x^2$ vs. $|t|$ at several fixed M_x^2 values. The data are obtained at 160, 270, 340 and 400 GeV/c and normalized to 300 GeV/c according to Eq. 5.

Figure 7: Parameter b vs. M_x^2 determined in the interval $0.003 \leq |t| \leq 0.017\ (\mathrm{GeV/c})^2$ by the fit

$$d^2\sigma/dtdM_x^2(M_x^2,t) = A(M_x^2)\exp(b(M_x^2)(t + 0.01))$$

The solid line corresponds to Eq. 9.

(The data are normalized to 300 GeV/c).

Figure 8: Parameter $A(M_x^2)$ (see the caption of Fig. 7) or the value of $d^2\sigma/dtdM_x^2$ vs. M_x^2 at $|t| = 0.01$ $(GeV/c)^2$. The solid line corresponds to Eq. 7. (The data are normalized to 300 GeV/c).

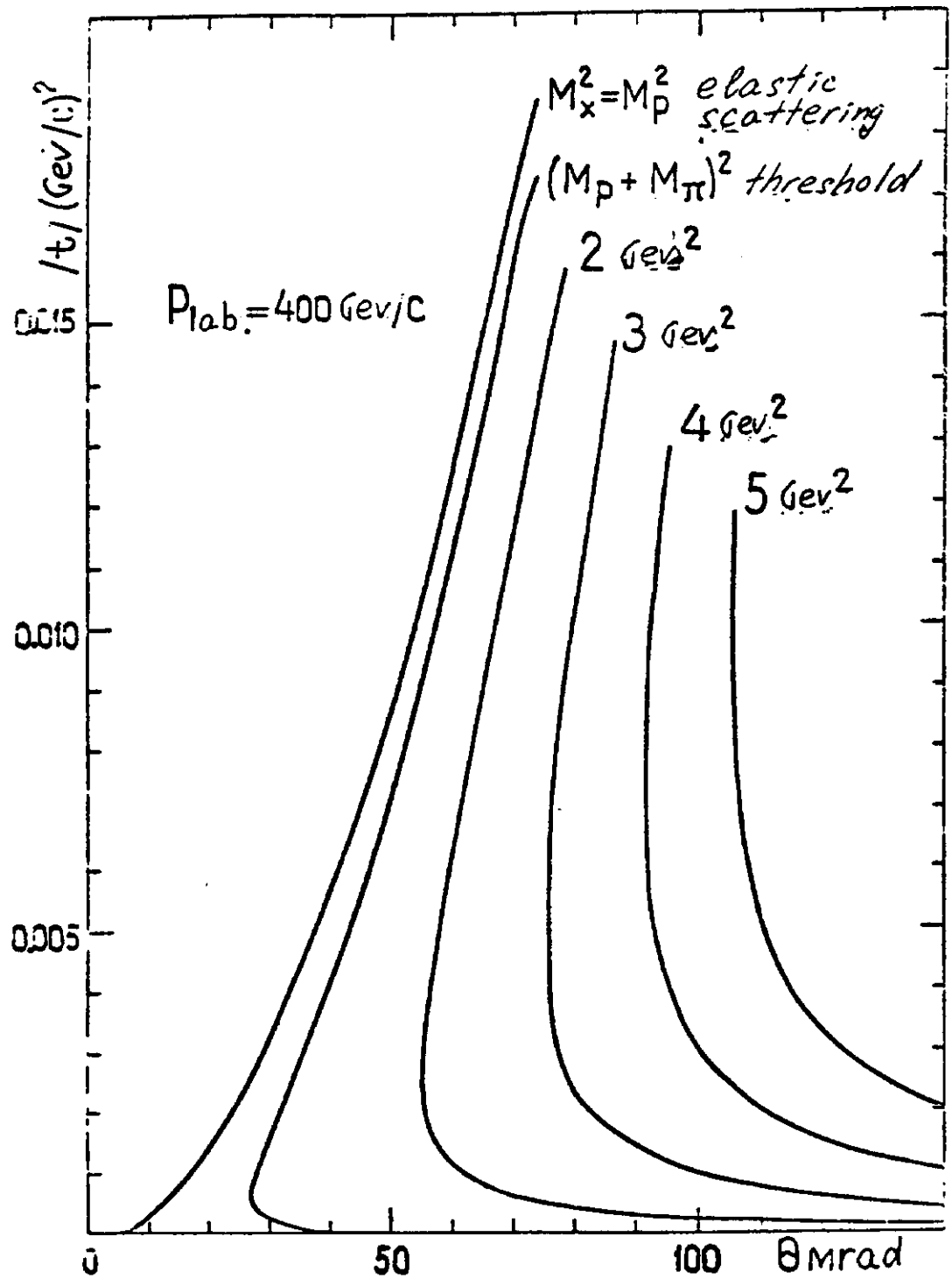
$|t|$ (Gev/c)^2
0.015
0.010
0.005
0
50
100
θ mrad
P_{lab} = 400 Gev/c
$M_x^2 = M_p^2$ elastic scattering
$(M_p + M_\pi)^2$ threshold
2 Gev^2
3 Gev^2
4 Gev^2
5 Gev^2

Fig. 1

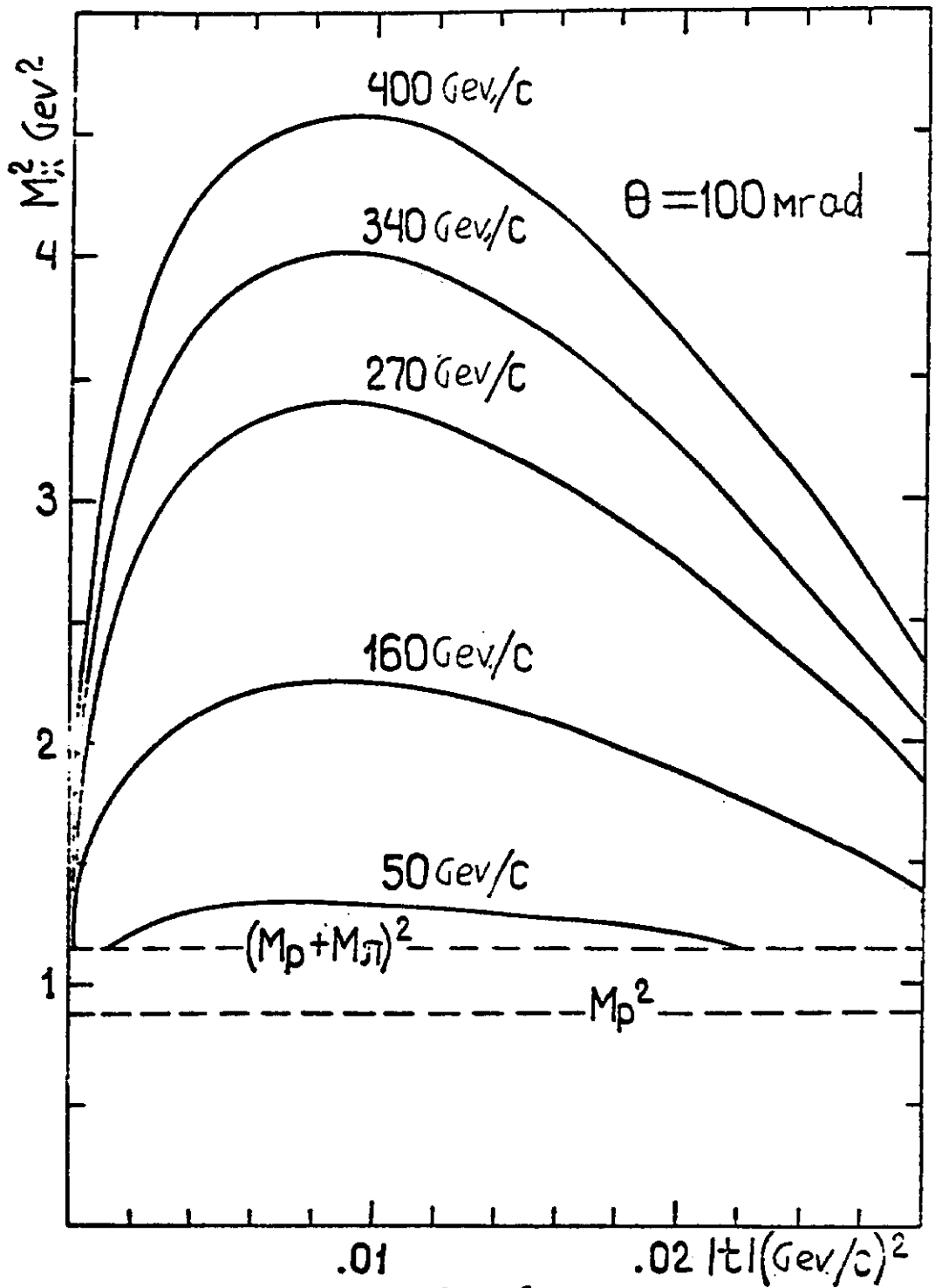
M_x^2 Gev^2
400 Gev/c
340 Gev/c
270 Gev/c
160 Gev/c
50 Gev/c
θ = 100 mrad
$(M_p+M_\pi)^2$
M_p^2
4
3
2
1
.01
.02 |t| (Gev/c)^2

Fig. 2

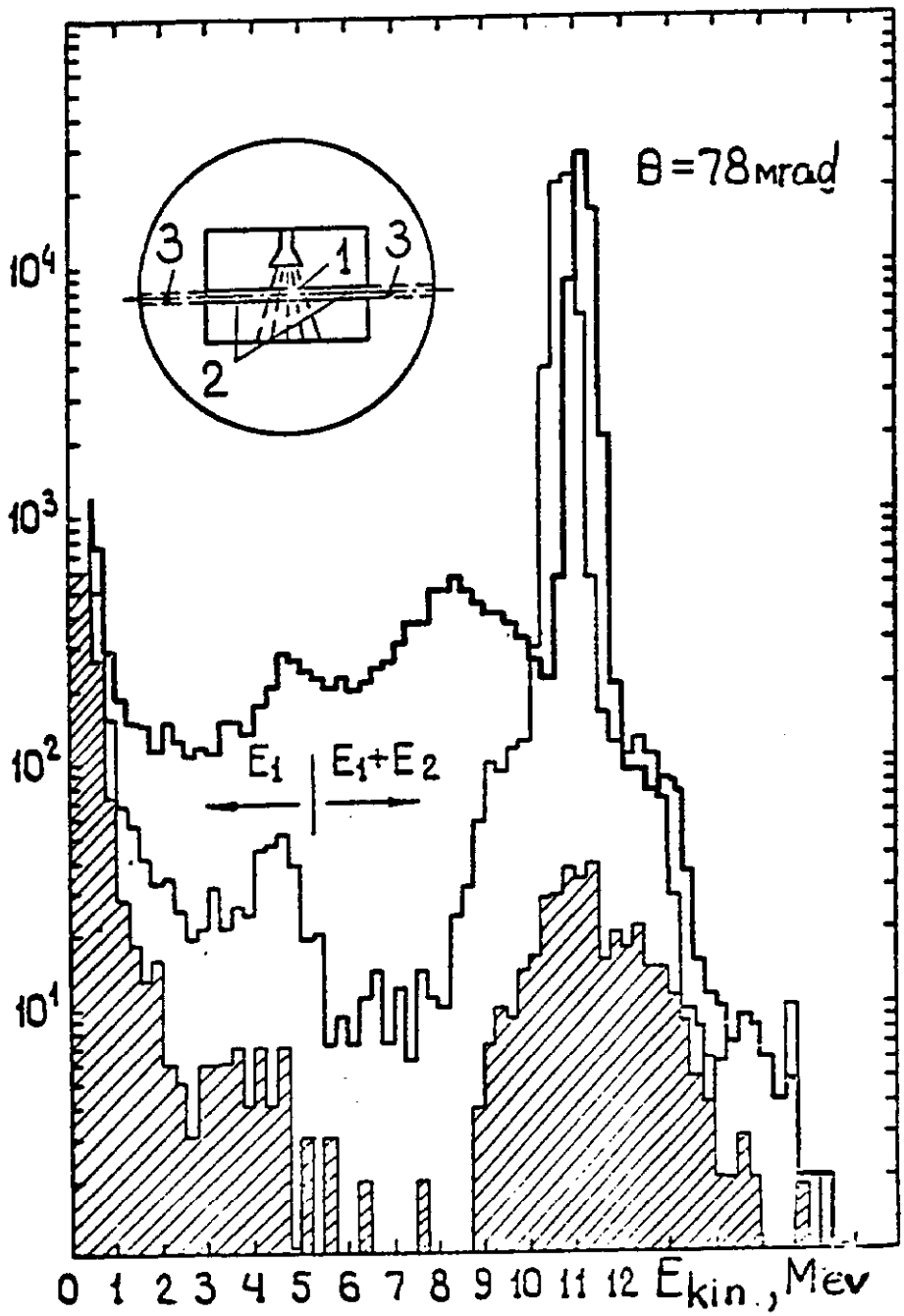
θ=78 mrad
3
1
3
2
10^4
10^3
10^2
10^1
E_1
E_1+E_2
0 1 2 3 4 5 6 7 8 9 10 11 12 $E_{kin.}$, Mev

Fig. 3

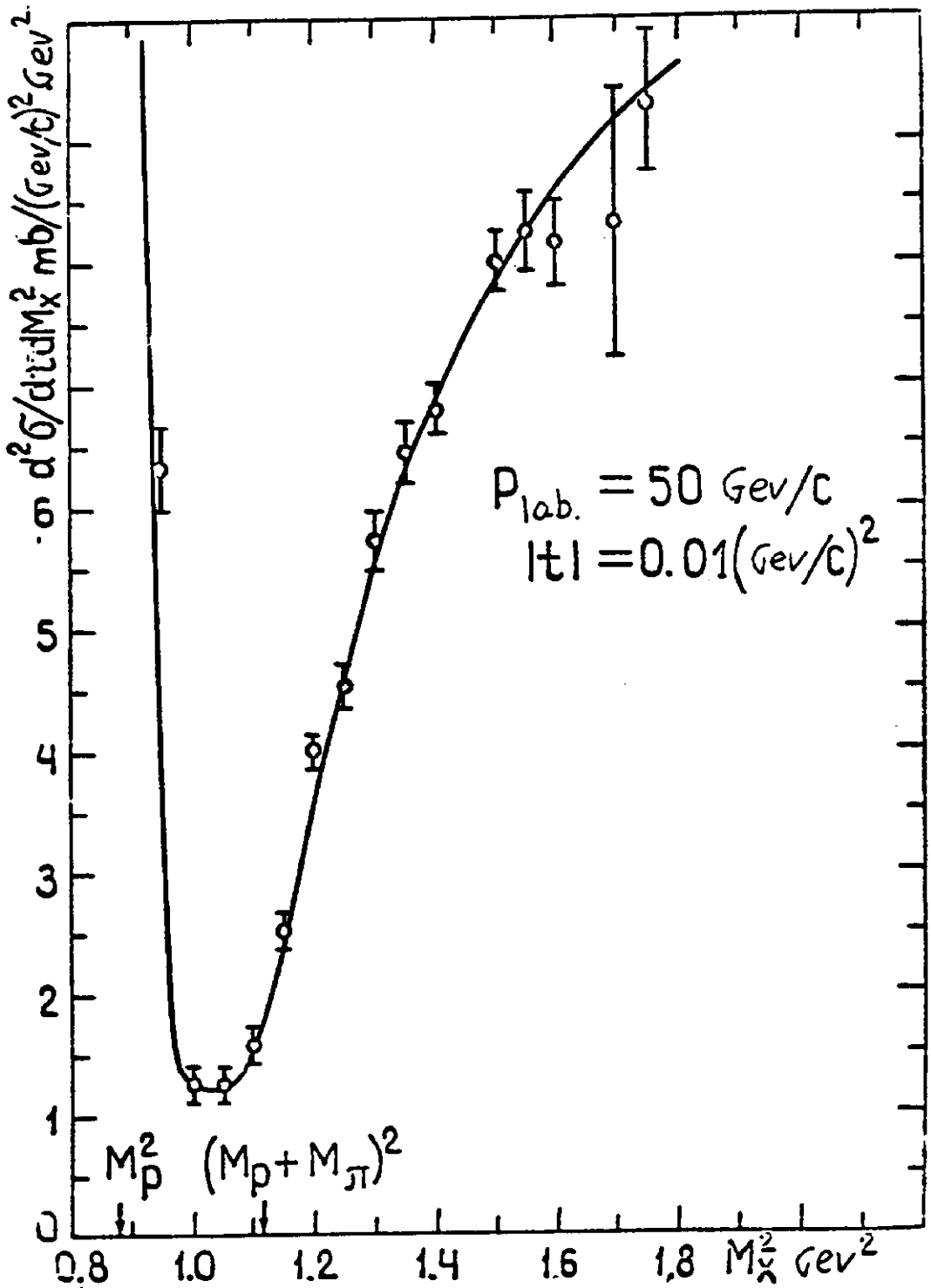
$d^2\sigma/dtdM_x^2$ mb/(Gev/c)^{2}Gev^2
$P_{lab.} = 50$ Gev/c
$|t| = 0.01$(Gev/c)^2
M_p^2
$(M_p + M_\pi)^2$
0
1
2
3
4
5
6
0.8
1.0
1.2
1.4
1.6
1.8
M_x^2 Gev^2

Fig. 4

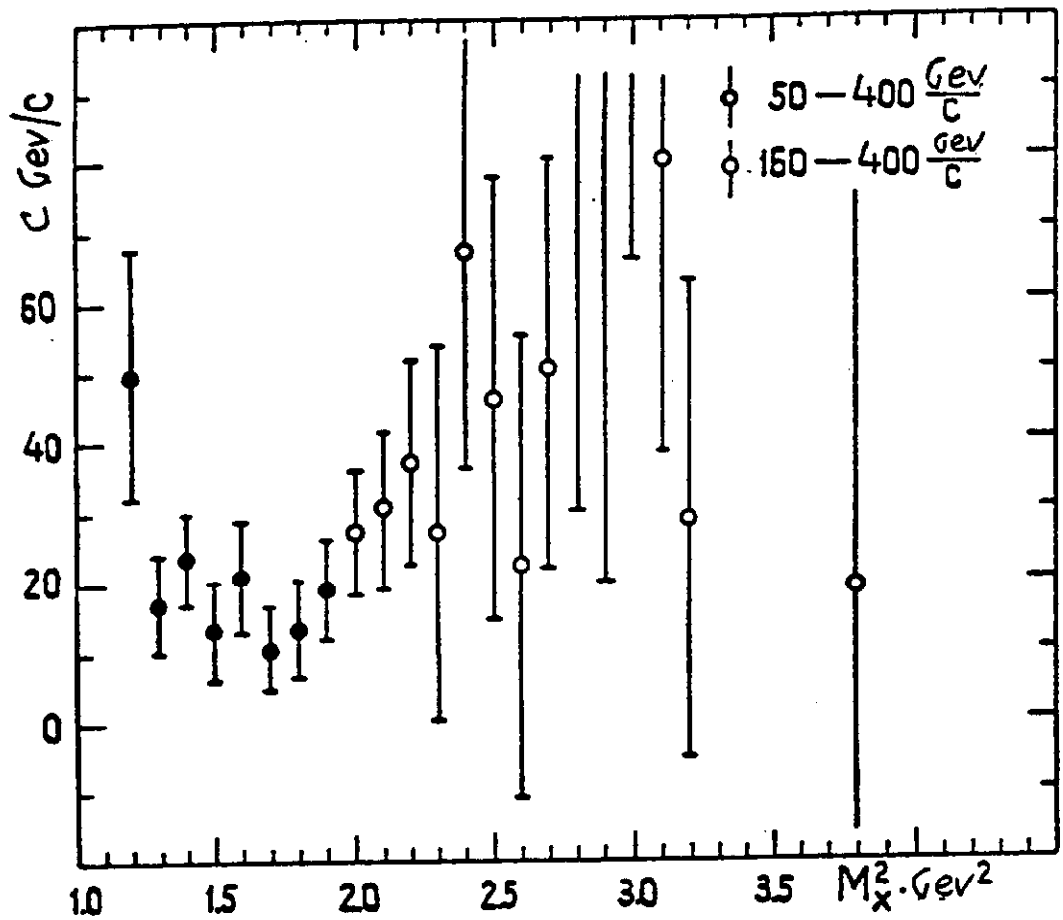
C Gev/c
60
40
20
0
1.0
1.5
2.0
2.5
3.0
3.5
$M_x^2 \cdot Gev^2$
50 — 400 Gev/c
150 — 400 Gev/c

Fig. 5

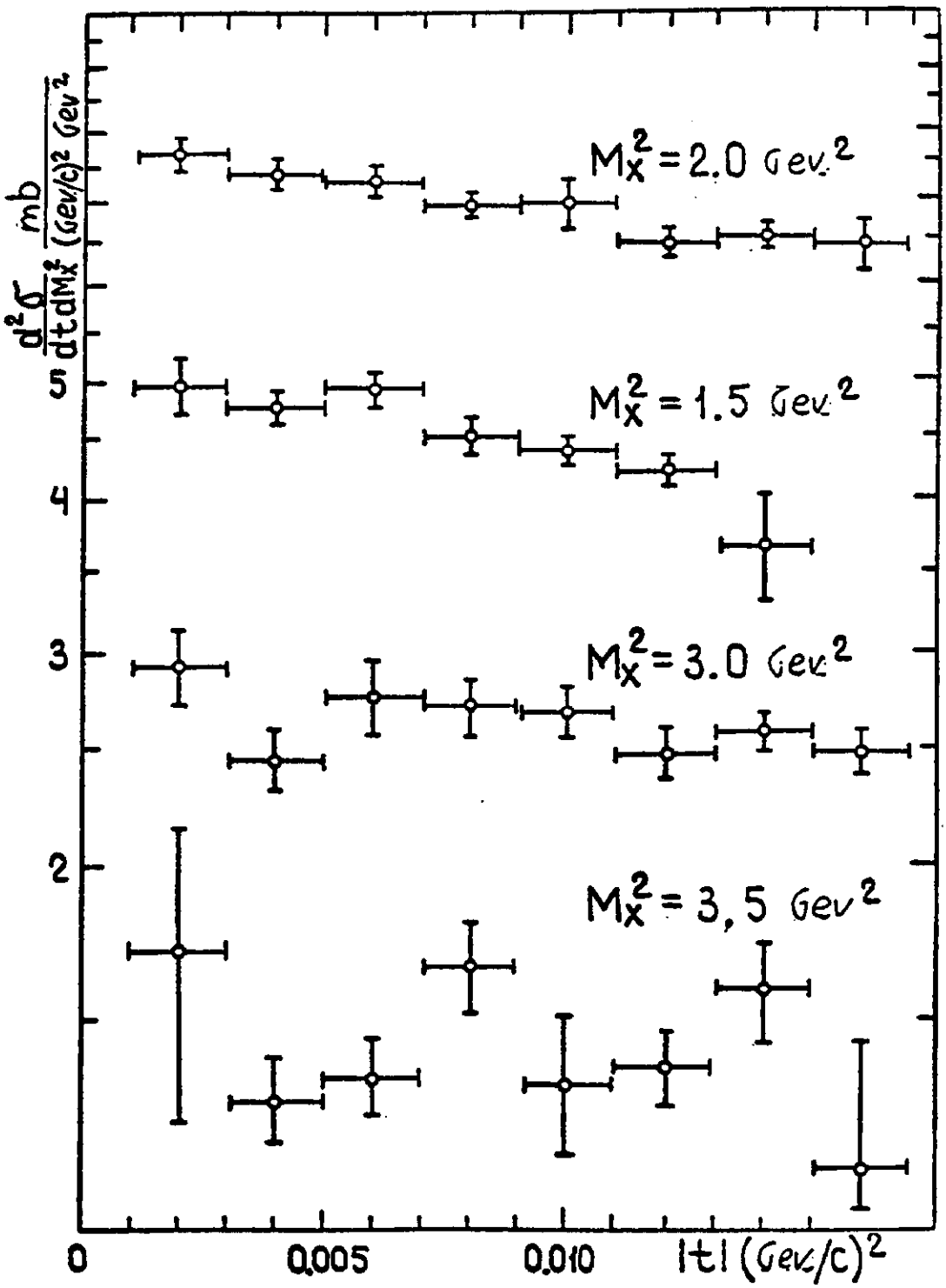
$\frac{d^2\sigma}{dt\,dM_x^2}$ $\frac{mb}{(Gev/c)^2\ Gev^2}$
$M_x^2 = 2.0$ Gev.^{2}
$M_x^2 = 1.5$ Gev.^{2}
$M_x^2 = 3.0$ Gev.^{2}
$M_x^2 = 3,5$ Gev^2
5
4
3
2
0
0.005
0.010
$|t|$ (Gev/c)^2

Fig. 6

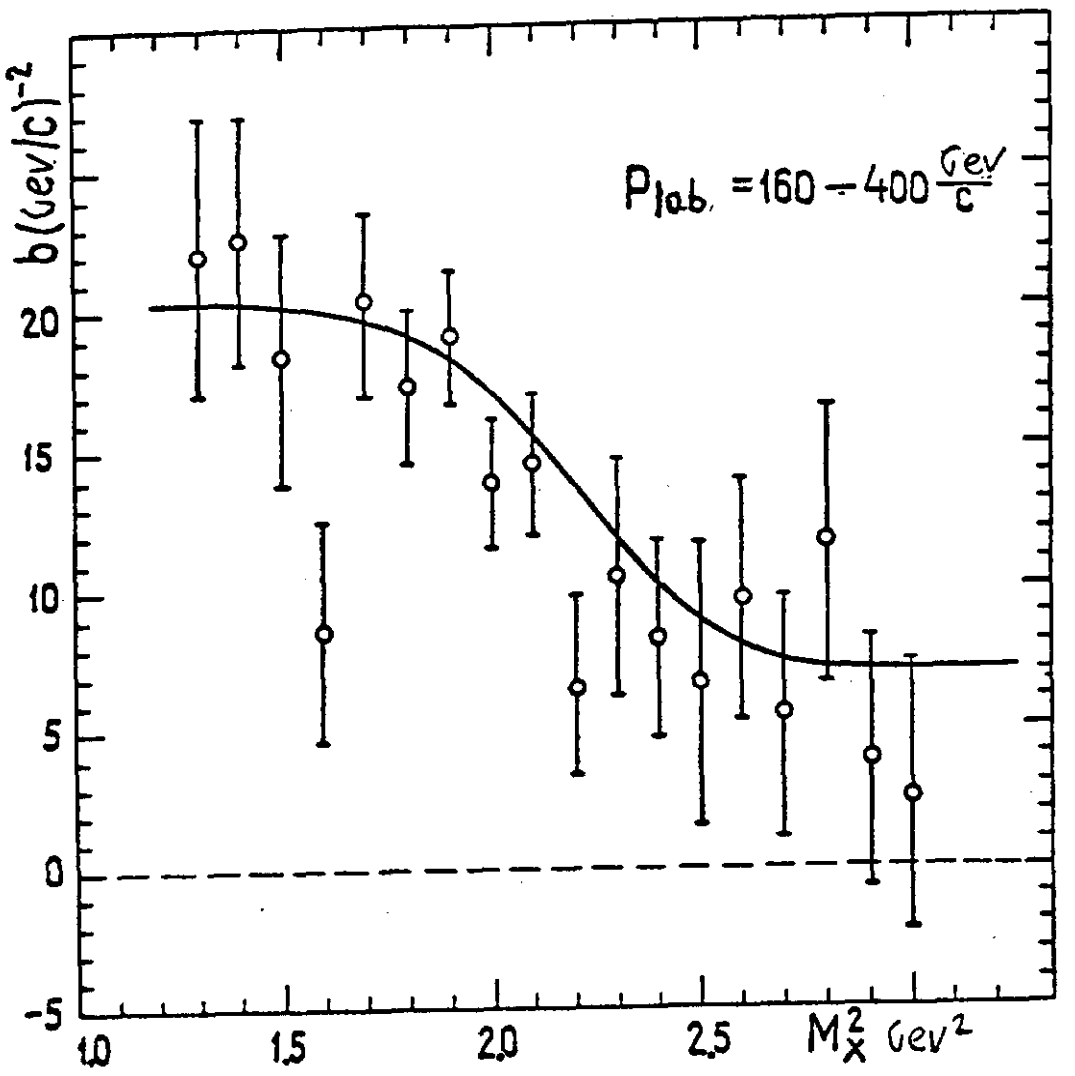
b (Gev/c)$^{-2}$
$P_{lab.} = 160 \div 400 \frac{Gev}{c}$
20
15
10
5
0
-5
1.0
1.5
2.0
2.5
M_X^2 Gev^2

Fig. 7

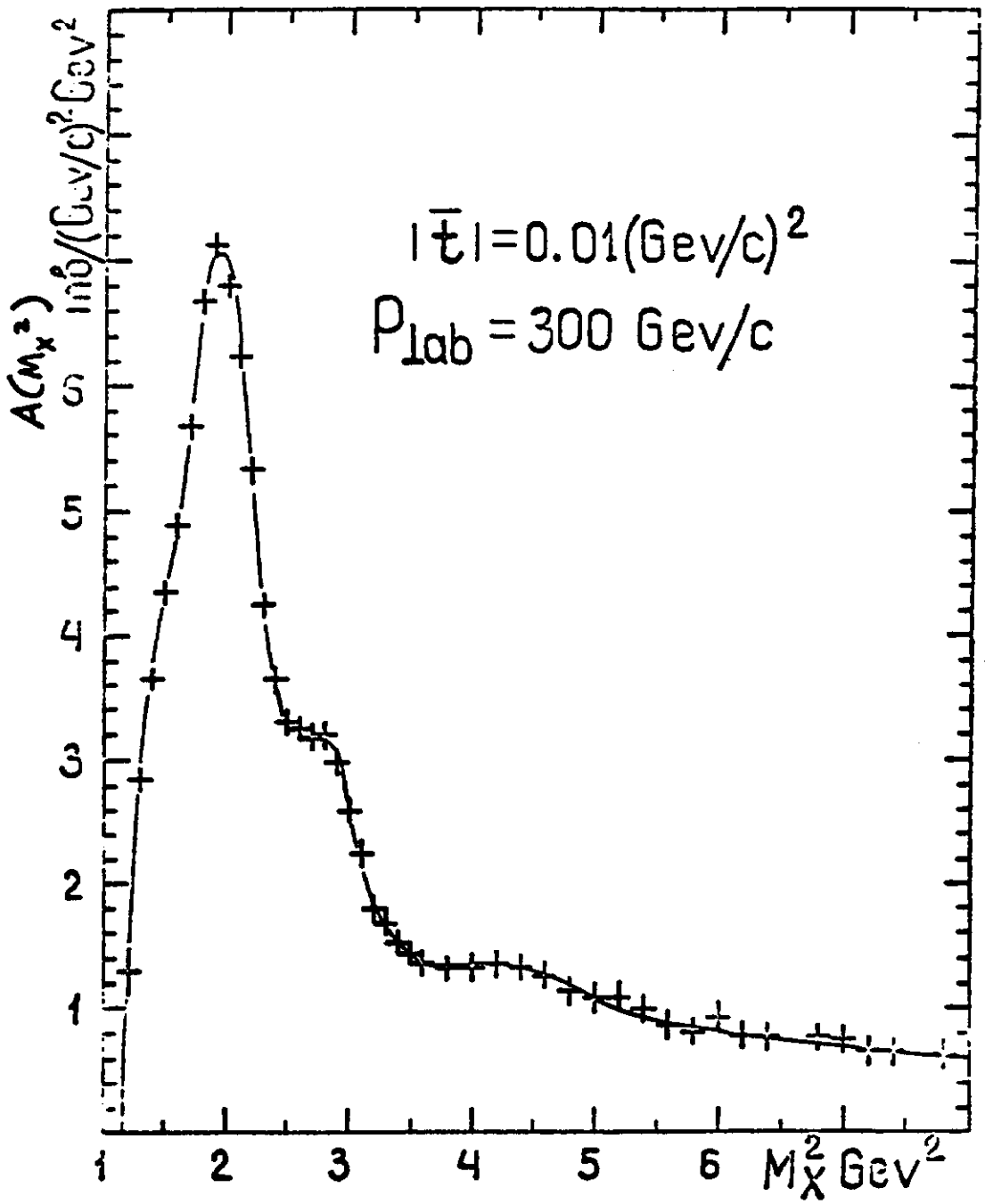
$A(M_x^2)$ mb/(Gev/c)^2·Gev^2
$|\bar{t}|=0.01$(Gev/c)^2
$P_{lab}=300$ Gev/c
1
2
3
4
5
6
M_X^2 Gev^2

Fig. 8